Dynamic Light Scattering of short Au–Rods with low aspect Ratio

Jessica Rodríguez-Fernández, Jorge Pérez–Juste, Luis M. Liz–Marzán, Peter R. Lang[†]

Departamento de Química Física and Unidad Asociada

CSIC- Universidade de Vigo, 36310, Vigo, Spain

[†] *Forschungszentrum Jülich, Institut für Festkörperforschung;*

Weiche Materie, D–52425 Jülich, Germany

Abstract

The translational and rotational diffusion of a series of gold nanorods with low aspect ratio was investigated by dynamic light scattering (DLS). It is shown that the translational and the rotational diffusion coefficient can be determined because the particle shape causes an anisotropy of the polarizability. This gives rise to two clearly distinguishable relaxation modes in the time correlation function of the scattered light. The particle length and aspect ratio were determined independently by transmission electron microscopy (TEM). Using a hydrodynamic model, these geometrical parameters were converted to diffusion constants, which agree well with the values determined by DLS. Additionally it is possible to obtain an estimate of the particles aspect ratio from the amplitude ratio of the two relaxation modes.

1

Introduction

Metal nanoparticles have received a great deal of attention since the early times of Colloid Science, when Michael Faraday first observed the range of different colours that gold colloids display as a function of size [1]. Since then, a plethora of studies have dealt with the production and characterization of noble metal colloids in a wide range of sizes [2–4], and for a variety of applications, including catalysis [5], biolabelling [6], biosensing [7], optical switches [8], among others. Only recently, variations in nanoparticle shape have been recognized as having a strong impact on their properties, which has motivated the development of synthetical methods for the preparation of particles with various geometries, such as rods [9–13], wires [14–16], prisms [17–21], cubes [22–24] and other polyhedrons [25, 26]. Most of these methods are based on wet chemistry reactions involving the reduction of metal salts and the adsorption of surfactants or other molecules, generally known as capping agents. The mechanisms directing the growth of particles with a particular geometry are still a matter of debate for most systems, but what is general is that they involve the growth of pre-existing nuclei in solution and this leads to a random process that implies that all particles are different, even in the most monodisperse samples. The characterization of the dimensions for such a variety of shapes is usually carried out using electron microscopy (EM), which implies the measurement of a large number (typically >100) of particles followed by averaging. This provides values for average dimensions and polydispersity (usually as standard deviation), but still is only representative of a limited population within the sample, and therefore may not provide the real size distribution of the whole sample. Additionally, EM measurements are carried out on dry samples, under vacuum and irradiating the specimen with high energy electron beams, which very likely affect the morphology and dimensions of the particles. We have been working on gold nanorods for several years now,

with the objective to understand the mechanism underlying their formation [13, 27, 28] as well as to understand and manipulate their extremely interesting, surface plasmon-related optical properties [29–31].

In this context, we have identified the need to apply alternative characterization techniques which overcome the mentioned drawbacks, i.e. techniques which probe a larger amount of particles, do not require solvent evaporation, and do not modify the particles themselves. Such requirements are fulfilled by scattering methods, which have been widely and successfully used for other colloidal systems. Among the various scattering techniques, light scattering is the one requiring a simpler setup and therefore it is available at many laboratories. However, its use to characterize metal colloids in general and gold nanorods in particular has not been very popular because of heating problems derived from absorption of the laser beam, limited applicability of the Rayleigh-Gans-Debye approximation, small particle sizes, and because models to analyze data for non-spherical particles seemed complicated. In the literature dealing with dynamic light scattering of rod like particles, very often the limiting case of rods with negligible anisotropy of the polarizability is considered, where different scenarios have to be applied depending on the rod length, L. For systems where the product of the scattering vector magnitude and rod length $QL \lesssim 5$ a single–exponential decay of the correlation function of the scattered intensity $g_2(t)$ (ITCF) is expected, provided the rods are fairly monodisperse in length. In the case where $QL > 10$ additional relaxation modes are observed in the correlation function. However, these cases are not relevant for our systems, because (i) the anisotropy of the polarizability of gold nanorods is not negligible, especially for particles with low aspect ratio [33], and (ii) the length of the rods in our case lies typically in the 50 nm range, i. e. $QL \lesssim 1$. Nevertheless we clearly observed two relaxation modes in the ITCF. To our knowledge, two relaxation modes in

the correlation function from rods smaller than 50 nm in length have been reported only once [34], in a fluorescence correlation spectroscopy (FCS) experiment. However, in that case the relaxation times of the relaxation mode which is ascribed to the translational diffusion is larger by two orders of magnitude than in our case, even though the particles are of comparable size. We therefore conjecture that long time diffusion has been observed in that case, while we are investigating short time Brownian dynamics. Thus, the unexpected appearance of two relaxation modes requires a thorough analysis.

An expression for the time auto correlation function for the scattered field can be extracted from the seminal work by Pecora [35], who showed that the spectral density of the scattered light can be expressed as the sum of an isotropic and an anisotropic contribution. Fourier transforming the spectral density gives the time dependence of the field auto correlation function, from which $g_2(t)$ can be calculated using the Siegert relation. By non–linear least squares fitting of this expression to our experimental data we determined the averaged translational, $\overline{D}$, and the rotational, D_r, diffusion coefficient of the Au–rods. Further we could obtain an estimate of the particle aspect ratio from the relative amplitudes of the ITCF. The paper is structured as follows. We describe the Au–rod synthesis, as well as the data acquisition and analysis procedures in the experimental section, while the results from dynamic light scattering are discussed and compared to transmission electron microscopy (TEM) data in the results and discussion section. Finally we append a brief derivation of the expression for the ITCF for the non-expert reader.

Experimental

Synthesis and characterization of Au–rods. A series of Au–nanorod samples (labelled as Au-1 to Au-5) with different aspect ratios were prepared through a seeding growth method first reported by Nikoobakht and El-Sayed [12] growing CTAB stabilized Au nanoparticle

seeds (<3 nm) by reduction of HAuCl$_4$ with ascorbic acid in the presence of a BDAC/CTAB mixture (in a 2.7 ratio) and a small amount of AgNO$_3$. The aspect ratio was varied through the amount of seed solution added (increasing from Au-1 to Au-5). Sample Au-6 was synthesized according to the modification of the seeding growth method reported by Liu and Guyot-Sionnest [32], where the reduction of HAuCl$_4$ with ascorbic acid on the pre-formed Au seeds in CTAB is carried out in the presence of HCl, to adjust the pH between 2 and 3. Tetrachloroauric acid (HAuCl$_4$·3H$_2$O), cetyltrimethylammonium bromide (CTAB), benzyldimethylammonium chloride (BDAC), ascorbic acid, sodium borohydride (NaBH$_4$), AgNO$_3$ and hydrochloric acid (HCl) were purchased from Aldrich and used as received. Milli-Q water with a resistivity higher than 18.2 M$\Omega\times$cm was used in all of the preparations.

Optical characterization was carried out by UV-visible-NIR spectroscopy with a Cary 5000 UV-Vis-NIR spectrophotometer, using 10 mm path length quartz cuvettes. Transmission electron microscopy (TEM) images from all samples were obtained with a JEOL JEM 1010 transmission electron microscope operating at an acceleration voltage of 100 kV. In the series from Au–1 through Au–5, the average aspect ratio of the particles was found to increase from 4.2 to 5.5, as expected from the synthesis conditions. For the sample Au–6 the aspect ratio is 4.2 (see Table I).

Dynamic Light Scattering. Sample solutions for light scattering were prepared from the original solution by repeated dilution steps with water, until the transmission of the solution and that of water could not be distinguished any more at a wavelength of $\lambda_0 = 647$nm. We further checked that additional dilution by a factor of two did not change the relaxation times of the time auto–correlation functions. In this case we may consider the solutions as infinitely dilute.

Time–autocorrelation functions of the scattered intensity $g_2(Q,t)$ were recorded with a

standard DLS apparatus equipped with a Kr–ion laser ($\lambda_0 = 647$nm) as a light source. The scattering angle, θ, was varied from 40º to 130º in steps of 10º, accordingly the scattering vector $Q = 4\pi n_s \sin(\theta/2)/\lambda_0$ covered a range of 8.835×10^{-3}nm $< Q < 2.43 \times 10^{-2}$nm. The polarization state of incident and scattered light was controlled with a $\lambda/2$-plate and a polarizer in the primary beam and an analyzer (all polarzing optics from Bernhard Halle Nachfl, Berlin Germany) in the scattered beam. The scattered light was collected with a monomode optical fiber (OZ-Optics, Ottawa, Canada) and detected with a SOSIP dual photomultiplier unit by ALV Laservertriebsgesellschft mbH, Langen, Germany. The TTL output of the avalanche diode was processed in the cross-correlation mode of a multiple tau correlator, ALV-5000. The shortest delay time which is reliably accessible with this detector–correlator combination is $\approx$ 100ns. For each sample, a complete angular set of correlation functions was recorded in both vertical–vertical (VV) and vertical–horizontal (VH) geometry.

Data analysis. For the particular case of small particles with cylindrical shape and non–negligible anisotropy of the polaraizability, expressions for the normalized intensity auto–correlation functions measured in the VH– and VV–geometry are given by

$$g_2^{VV}(Q,t) - 1 = \beta \left[A^2 \exp\left\{-\Gamma t\right\} + 2AB \exp\left\{-(\Gamma + \Delta/2)t\right\} + B^2 \exp\left\{-(\Gamma + \Delta)t\right\} \right] \quad (1)$$

$$g_2^{VH}(Q,t) - 1 = \beta' \exp\left\{-(\Gamma + \Delta)t\right\} \quad (2)$$

respectively. Here $\Gamma = 2\overline{D}Q^2$ and $\Delta = 12D_r$, while $A + B = 1$ (see apendix for details). The parameters β and β' describe the non—ideal dynamical contrast of the light scattering set up, and are slightly less than unity. According to eqs. 1 and 2 the standard procedure to determine $\overline{D}$ and D_r is to plot the relaxation rate of $g_2^{VH}(t) - 1$ vs. Q^2. The intercept of the resulting linear relation is $12D_r$ and the slope is $2\overline{D}$. Furthermore, a plot of the

relaxation rate of $g_2^{VH}(t \gg 1/6D_r) - 1$ gives a linear relation with a slope of $2\overline{D}$ and zero intercept. We decided not to use this procedure for three reasons. First, the choice of the threshold $t \gg 1/6D_r$ could not be determined unambiguously from our data. Second, as will turn out, the relaxation rate of $g_2^{VH}(t) - 1$ does not depend significantly on the scattering vector. This implies that $6D_r \gg \overline{D}$ and that $\overline{D}$ cannot be determined with high reliabilty from either of the two mentioned possibilities. Third, the determination of the relaxation rates requires some kind of least squares fitting in any case. We therefore chose to non–linear least squares fit the entire ITCFs by eqs. 2 and 1 to determine D_r and $\overline{D}$. This has the further advantage that also the amplitudes of the two relaxation modes can be determined, which carry information on the aspect ratio of the particles. To achieve the highest possible reliability of the best fitting parameters, we applied a global fitting algorithm, in which we analyzed the complete set of of correlation functions obtained from one sample simultaneously. In his procedure A, $\overline{D}$ and D_r were treated as global parameters, while β and β' were allowed to vary between different correlation functions.

Results and Discussion

The choice of samples for the measurements was based on a compromise among various parameters. First, we intended to achieve a reasonably wide range of aspect ratios, and whenever possible of particle size. However, in order to avoid excessive absorption of the incident laser beam (647 nm), which would lead to significant local heating, the corresponding transverse and longitudinal surface plasmon absorption bands should be located below and above this wavelength, respectively. Another constraint was the need for the highest monodispersity achievable in practice, which is mainly restricted to aspect ratios below 6. Since low aspect ratios would involve high absorption at the wavelength of interest and high aspect ratios lead to high polydispersity, we decided to concentrate on a relatively narrow
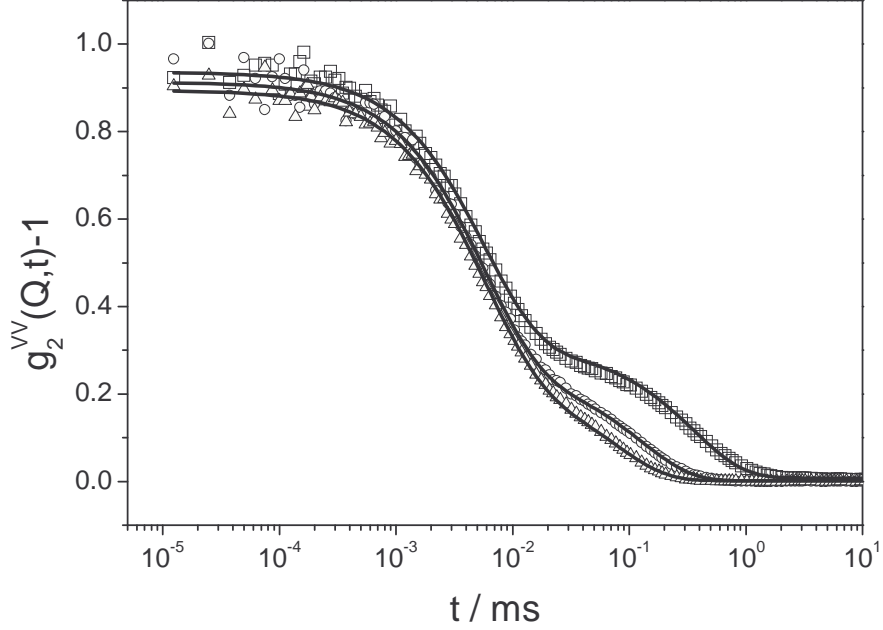
FIG. 1: ITCF from the sample Au–1 recorded in the VV-geometry. Different symbols refer to different scattering angles. For the sake of clarity only three out of ten curves are displayed, i. e. 40º (□), 90º (○) and 130º (△). Full lines are non linear least squares fits according to eq. 1

range of aspect ratios between 4.2 and 5.5. As described in Table 1, for aspect ratios between 4.4 and 5.5, the nanorod average length was maintained approximately constant, with a systematic variation of the width, while for aspect ratio 4.2, two relatively different dimensions were selected. The UV-vis-NIR spectra for all samples are shown in the Supporting Information, together with representative TEM images.

Intensity auto–correlation functions (ITCF) obtained from the sample Au–1 recorded in VV–geometry are displayed in Fig. 1. For clarity we have plotted only the curves from three different scattering angles, namely 40º, 90º and 130º. It can be clearly seen that at all different angles there are two relaxation modes, one of which becomes faster with increasing θ, and one which is virtually independent of the scattering angle. Similarly the relaxation times of the ITCF recorded in VH–geometry do not change with scattering angle. This is
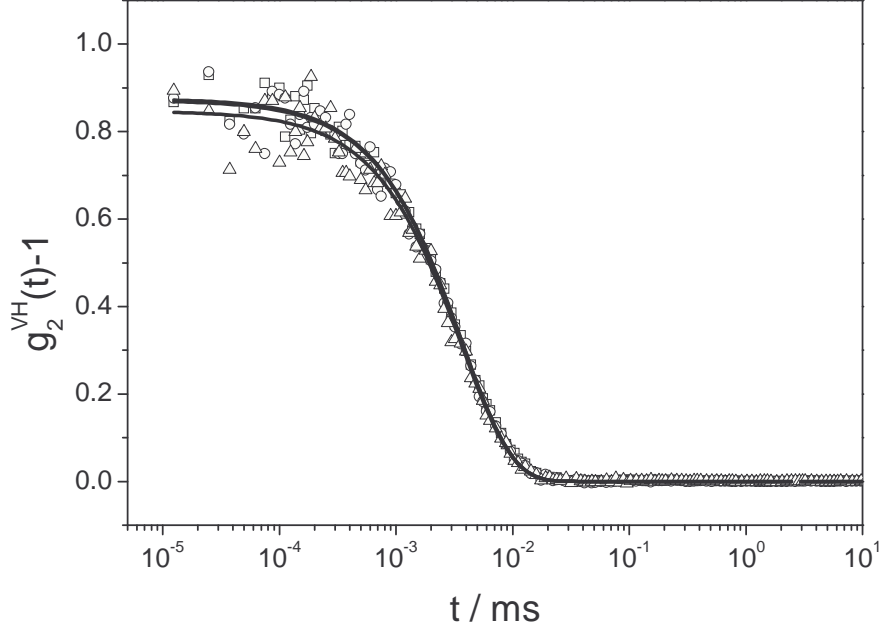
FIG. 2: ITCF from the sample Au–1 recorded in the VH-geometry. Different symbols refer to different scattering angles. For the sake of clarity only three out of ten curves are displayed, i. e. 40º (□), 90º (○) and 130º (△). Full lines are non linear least squares fits according to eq. 2

shown for the sample Au–1 in Fig. 2. This behavior is not expected at first glance from eqs. 1 and 2, since all exponentials in these equations have relaxation rates which are linearly proportional to Q^2. On the other hand, if $\overline{D}Q^2 \ll D_r$ only the first term of eq. 1 depends significantly on the scattering angle. This means that the slow relaxation mode in the VV correlation functions is related to the translational diffusion of the rods alone while the fast mode and the relaxation rates of the VH correlation functions are dominated by rotational diffusion. Global fitting of the experimental ITCF as described in the experimental section yielded the parameters listed in Table I. In this table we also list the geometrical particle parameters, L and L/D_{cs} obtained from the analysis of TEM micrographs. The deviations listed together with the data are reliability intervals from the fitting routine in case of the diffusion coefficients. In the case of the parameters from TEM they represent standard

TABLE I: Mean translational, $\overline{D}$, and rotational, D_r, diffusion coefficients measured by DLS of gold rods in suspension, and rod lengths L as well as aspect ratios, L/d_{cs} from TEM.

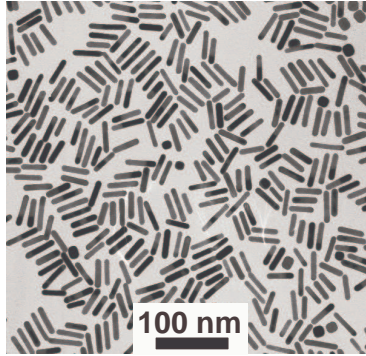| sample	$\overline{D}$	D_r	L	L/d_{cs}
	$\mathrm{nm^2/ms}$	$\mathrm{ms^{-1}}$	nm	
Au–1	12200± 200	23.2± 0.6	45.9±6.3	4.2±1.1
Au–2	14100± 400	29.7± 0.3	38.2±5.9	4.4±0.9
Au–3	15200± 600	36.5± 1.2	38.4±5.0	4.6±1.0
Au–4	16300± 600	47.3± 0.9	37.5±5.4	5.2±1.1
Au–5	19000± 500	52.6± 0.3	37.3±5.7	5.5±1.2
Au–6	7100± 400	8.3± 0.7	60.6±10.4	4.2±0.8

FIG. 3: TEM micrograph of sample Au–4.

deviation of the distribution of the corresponding parameter. As a representative example we show a TEM-picture in Fig. 3

This micrograph shows that the rods have relatively narrow distribution both in length and aspect ratio, which is confirmed by the standard deviations of the corresponding distributions, which are in the range of 15 % for the length and about 10% for the aspect ratio. We also observe a small number of cubes, which is a general finding in these samples.

However, their relative amount is very low and thus they are not expected to contribute significantly to the global scattering of the sample. Therefore we will consider the rods to be monodisperse in the following discussion. A first approximation for the relation between geometrical parameters and diffusion constants of colloidal rods has been given by Brørsma [36, 37], which however is sufficiently accurate only for rods with $\ln(L/d_{cs}) > 2$. Since this requirement is not fulfilled for our Au–rods, we chose to apply the expression by Ortega and de la Torre [38]

$$
\begin{aligned}
\overline{D} &= \frac{k_B T (\ln(L/d_{cs}) + \overline{C})}{3\pi\eta L} \\
D_r &= \frac{3k_B T (\ln(L/d_{cs}) + C_r)}{\pi\eta L^3}.
\end{aligned}
\tag{3}
$$

Here $\overline{C}$ and C_r are second order polynomials in d_{cs}/L, the coefficients of which have been determined by fitting of numerical data.

$$
\begin{aligned}
\overline{C} &= 0.312 + 0.565\frac{d_{cs}}{L} - 0.100\left(\frac{d_{cs}}{L}\right)^2 \\
C_r &= 0.662 + 0.917\frac{d_{cs}}{L} - 0.05\left(\frac{d_{cs}}{L}\right)^2.
\end{aligned}
\tag{4}
$$

These equations apply to our particles, because they were derived for the ranges of $2 < L/d_{cs} < 20$. In Table II we compare the diffusion coefficients measured by DLS with those calculated with eqs. 3 and 4. Reasonable agreement between the experimental and the calculated values could only be achieved by considering a double-layer of CTAB around the rods, which stabilizes the particles by exposing the charged ammonium groups to the polar solvent [39, 40] The thickness of this bilayer was estimated to be ca. 4 nm according to the standard rule of thumb for the contour length of an alkane chain, i. e. $l_c = n \times 0.126 + 0.154$ nm [41], where n is the number of carbon atoms in the chain. A similar effect was observed by van der Zande et al [42] for long gold rods (typically $L > 200$ nm and $L/d_{cs} > 10$) which were sterically stabilized by an adsorbed polymer layer. These authors found

TABLE II: Mean translational, $\overline{D}$, and rotational, D_r, diffusion coefficients measured by DLS, and corresponding values, $\overline{D}^*$ and D_r^*, calculated by using eqs. 3 through 4 and the geometrical parameter listed in Table I. In addition, a stabilizing surfactant layer of 4 nm thickness was accounted for.

sample	$\overline{D}$	D_r	$\overline{D}^*$	D_r^*
	$\mathrm{nm}^2/\mathrm{ms}$	ms^{-1}	$\mathrm{nm}^2/\mathrm{ms}$	ms^{-1}
Au–1	12200	23.2	13900	19.4
Au–2	14100	29.7	16000	30.1
Au–3	15200	36.5	16200	30.4
Au–4	16300	47.3	17000	34.2
Au–5	19000	52.6	17300	35.4
Au–6	7100	8.3	11400	10.1

that the translational diffusion coefficients were up to a factor of four smaller than those expected from the particles geometrical parameters. For the rotational diffusion coefficient the discrepancy could even amount to almost an order of magnitude. This discrepancy was assigned to the stabilizing polymer layer, which in this case had a thickness comparable to the particles cross sectional diameter.

In the present study we find agreement between the calculated and the experimental values within less than 20% for the rotational diffusion coefficient of the particles with an aspect ratio smaller than 5. Only for the two samples with the largest aspect ratios the discrepancy is ca. 30%. In the case of $\overline{D}$ the agreement is better than 15 % in most cases with a slight tendency to decrease with increasing aspect ratio of the rods. This is probably due to the fact that the theory by Ortega and Garcia de la Torre was devised for cylinders

with flat base areas while our gold rods are more of spherocylindrical shape, as can be seen from Fig. 3. Intuitively one would expect this effect to become smaller with increasing aspect ratio of the rods.

As mentioned above, it is possible to obtain information on the particle aspect ratio from the ratio of the relative amplitudes A/B of the two relaxation modes measured in $VV-$ geometry. This will be discussed in detail in the following. According to Pecora [35] the ratio of the amplitudes is related to the components of the polarizability tensor by

$$\frac{A}{B} = \frac{5}{4} \frac{\alpha_I^2}{\langle (\alpha_\perp - \alpha_\parallel)^2 \rangle},$$

where $\parallel$ denotes the direction parallel to the rod's long axis and $\perp$ the direction normal to it. On the other hand, if the particle size is small compared to the wavelength, the dipole approximation applies [43]. In this case Rayleigh's theory [44] for the polarizability of ellipsoids is commonly used to estimate the polarizability of the rods [45]. Applying this approximation is necessary because there is no theoretical expression for rods available. According to Rayleigh, the polarizability of an ellipsoid in the direction of one of the symmetry axes is

$$\alpha_j = V \frac{\epsilon - \epsilon_m}{\epsilon_m + L_j(\epsilon - \epsilon_m)} \tag{5}$$

where V is the volume of the ellipsoid, $\epsilon = \epsilon' + \imath\epsilon''$ is the complex dielectric function of the ellipsoid material at a given wavelength, ϵ_m is the dielectric constant of the solvent and $j =\parallel$ or $\perp$ denotes the axis of the ellipsoid. Note that the value of the dielectric function is the same for all axes and any anisotropy of the polarization is a mere geometrical effect
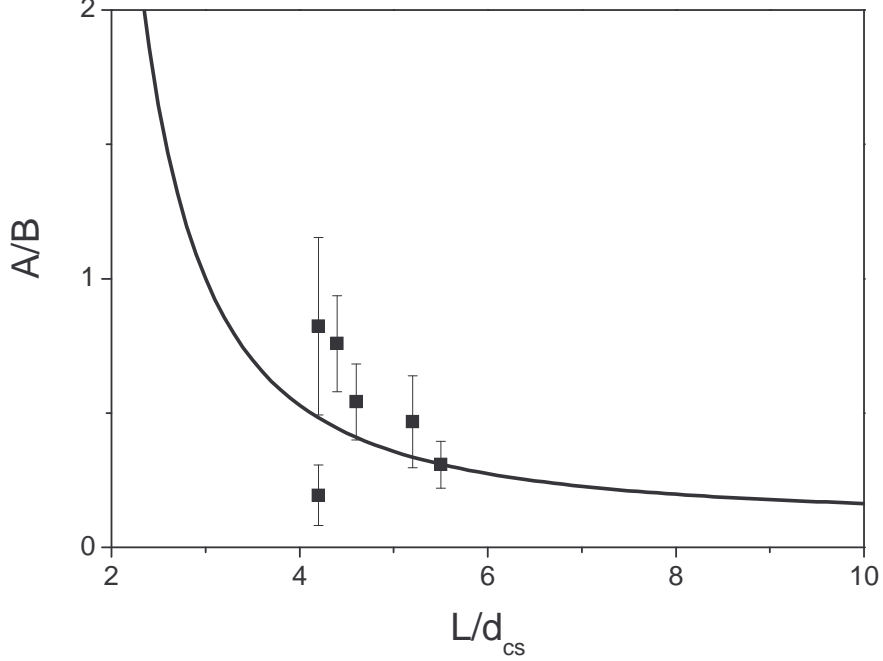
FIG. 4: Amplitude ratio of the relaxation modes in $g_2(t) - 1$ vs. aspect ratio. Symbols are experimental points as determined by DLS and TEM. The full line was calculated using eq. 8 which is due to the factors

$$L_{\parallel} = \frac{1 - e^2}{e^2} \left(\frac{1}{2e} \ln \frac{1 + e}{1 - e} - 1 \right) \tag{6}$$

$$Ł_{\perp} = \frac{1 - L_{\perp}}{2}. \tag{7}$$

for an ellipsoid of revolution, for which the two normal axes are equally long. The eccentricity of the ellipsoid is $e = \sqrt{(1 - (b/a)^2)}$ where a is the length of the rotation axis and b the length of the axis normal to that. To apply this formalism to approximate the properties of rods b/a has to be replaced by d_{cs}/L.

Thus,the amplitude ratio of the ITCF can be related directly to the aspect ratio and the dielectric function of the particle. After some straight forward algebra one obtains

$$\frac{A}{B} = \frac{5}{4} \frac{4\mathcal{M}_{\perp} + 2\mathcal{N}\mathcal{M}_{\parallel}\mathcal{M}_{\perp} + \mathcal{M}_{\parallel}}{\langle \mathcal{M}_{\perp} - \mathcal{N} + \mathcal{M}_{\parallel} \rangle}. \tag{8}$$

Here $\mathcal{M}_j = \left[(\epsilon_m + L_j\epsilon')^2 + L_j^2\epsilon''^2 \right]^{-1}$ and $\mathcal{N} = 2 \left[\epsilon_m^2 + \epsilon_m\epsilon'(L_{\perp} + L_{\parallel}) + L_{\perp}L_{\parallel}(\epsilon'^2 + \epsilon''^2) \right]$.

With this expression we calculated the dependence of A/B on the particle aspect ratio, which is shown in Fig. 4, together with the experimental data for A/B. For the values for the dielectric function of gold at $\lambda_0 = 647$ nm we used $\epsilon\prime = -12.789$ and $\epsilon\prime\prime = 1.116$ [46]and for the solvent we took the value of water $\epsilon_m = n^2 = 1.772$. We find good qualitative agreement between the calculated curve and the experimental data points. Generally the theoretical curve is lying below the data points with an increasing deviation towards smaller aspect ratios. This is probably due to the approximation of the rods' polarizabilty, by that of an ellipsoid. As the anisotropy of the polarizabilty is only due to the particle shape, this approximation is expected to hold better for larger aspect ratios. Further, the single data point which is lying below the theoretical curve corresponds to the sample Au–6, which is significantly longer than the others. This might lead to reduction of A due to the influence of the particle form factor $P(Q)$.

Generally the above calculations show that the amplitude of the relaxation mode which depends on the translational and the rotational diffusion coefficient, i. e. B become increasingly dominating with respect to A, if the particle aspect ratio exceeds a value of 10. This is obviously the reason why in the pioneering work by van der Zande et al [42] on dynamic light scattering of gold rods, a single relaxation process of the ITCF was observed. These authors had investigated only samples with $L/d_{cs} > 12$ with dynamic light scattering. They refrained from DLS measurements of the rods with smaller aspect ratios because of the high polydispersity of their samples[47].

Conclusions

The auto–correlation function of the scattered intensity recorded in VV–geometry from gold rods with small aspect ratio shows two distinct relaxation processes. Applying Pecora's expression for the correlation function we determined the translational and rotational diffu-

sion coefficients as well as the amplitudes of the individual relaxation modes. The diffusion coefficients are in good agreement with the values calculated from the geometrical parameters of the rods, if the thickness of the stabilizing surfactant bilayer is taken into account. Further, we presented a path to estimate the aspect ratio of the particles from the ratio of the relative amplitudes of the correlation function.

Acknowledgements

Appendix: Time auto–correlation function, $g_1(t)$, of the scattered field.

In reference [35] Pecora showed that the spectral density of scattered light can be written as the sum of an isotropic and an anisotropic contribution

$$I(Q,\omega) = I_{iso}(Q,\omega) + I_{aniso}(Q,\omega). \tag{9}$$

With

$$I_{iso}(Q,\omega) = \frac{\rho}{2\pi} K^2 \cos^2(\phi) \sin^2(\theta) \alpha_I^2 P(Q) S_{iso}(Q,\omega) \tag{10}$$

and

$$I_{aniso}(Q,\omega) = \frac{\rho}{30\pi} K^2 \left(3 + \cos^2(\phi)\sin^2(\theta)\right) S_{aniso}(Q,\omega) \tag{11}$$

where ρ is the particle number density, K is an optical contrast factor and $\alpha_I = (2\alpha_\perp + \alpha_\parallel)/3$. The angle between the wave vector of the scattered light and the polarization vector of the incident light is denoted θ, while ϕ is the angle between the polarizatoion vector of the scattered light and the plane span by the wave vector of the scattered light and the polarization vector of the incident light. Thus in VV–geometry $\cos^2(\phi)\sin^2(\theta) = 1$ and

$\cos^2(\phi)\sin^2(\theta) = 0$ in VH–geometry. The isotropic contribution to the dynamic structure factor is given by the Lorentzian

$$S_{iso}(Q,\omega) = \frac{2Q^2\overline{D}}{\omega^2 + (Q^2\overline{D})^2},\tag{12}$$

while the anisotropic contribution consists of a sum of five Lorentzians. For the particularly simple case of particles with cylindrical symmetry the latter reduces to

$$S_{aniso}(Q,\omega) = \frac{\langle\left(\alpha_\perp - \alpha_\parallel\right)^2\rangle}{3}\frac{2(Q^2\overline{D} + 6D_r)}{\omega^2 + (Q^2\overline{D} + 6D_r)^2},\tag{13}$$

According to the Wiener–Khinchin theorem, the time auto–correlation function of the scattered light is related by a Fourier transformation to the spectral density, thus

$$g_1(t) = \widetilde{S}_{iso}(Q,t) + \widetilde{S}_{aniso}(Q,t).\tag{14}$$

Consequently, we get for the normalized field auto-correlation function in VV–geometry

$$\widehat{g}_1^{VV}(t) = A\exp\left\{-\overline{D}Q^2 t\right\} + B\exp\left\{-(\overline{D}Q^2 + 6D_r)\right\},\tag{15}$$

with $A = \alpha_I^2/(\alpha_I^2 + \langle\left(\alpha_\perp - \alpha_\parallel\right)^2\rangle)$ and $B = \frac{4}{15}\langle\left(\alpha_\perp - \alpha_\parallel\right)^2\rangle/(\alpha_I^2 + \langle\left(\alpha_\perp - \alpha_\parallel\right)^2\rangle)$. The corresponding expression for VH–geometry is

$$\widehat{g}_1^{VH}(t) = \exp\left\{-(\overline{D}Q^2 + 6D_r)\right\}.\tag{16}$$

Applying the Siegert–relation gives the final expressions of eqs. 1 and 2 which we used as model functions for the analysis of our experimental data.

---

[1] Faraday, M. *Philos. Trans. Royal Soc. London* **1857**, *147*, 145.

[2] Frens, G. *Nature* **1973**, *241*, 20.

[3] Rodríguez-Fernández, J.; Pérez-Juste, J.; García de Abajo, F. J.; Liz-Marzán, L. M. *Langmuir* **2006**, *22*, 7007.

[4] Evanoff, D. D. Jr.; Chumanov, G. *J. Phys. Chem. B* **2004**, *108*, 13948.

[5] Toshima, N., *Metal nanoparticles for catalysis* in *Nanoscale Materials*; Kluwer Academic Publishers: Boston, 2003.

[6] Gittins, D. I.; Caruso, F. *Chem. Phys. Chem.* **2002**, *3*, 110.

[7] Lee, K.-S.; El-Sayed, M.A. *J. Phys. Chem. B* **2006**, *110*, 19220.

[8] Hu, M.-S.; Chen, H.-L.; Shen, C.-H.; Hong, L.-S.; Huang, B.-R.; Chen, K.-H.; Chen, L.-C.*Nature Mater.* **2006**, *5*, 102.

[9] van der Zande, B. M. I.; Boehmer, M. R.; Fokkink, L. G. J.; Schoenenberger, C. *J. Phys. Chem. B* **1997**, *101*, 852.

[10] Chang, S.-S.; Shih, C.-W.; Chen, C.-D.; Lai, W.-C.; Wang, C. R. C. *Langmuir* **1999**, *15*, 701.

[11] Busbee, B. D.; Obare, S. O.; Murphy, C. *J. Adv. Mater.* **2003**, *15*, 414.

[12] Nikoobakht, B.; El-Sayed, M. A. *Chem. Mater.* **2003**, *15*, 1957.

[13] Pérez-Juste, J.; Liz-Marzán, L. M.; Carnie, S.; Chan, D. Y. C.; Mulvaney, P. *Adv. Funct. Mater.* **2004**, *14*, 571.

[14] Sun, Y.; Gates, B.; Mayers, B.; Xia, Y. *Nano Lett.* **2002**, *2*, 165.

[15] Sun, Y.; Yin, Y.; Mayers, B. T.; Herricks, T.; Xia, Y. *Chem. Mater.* **2002**, *714*, 4736.

[16] Vasilev, K.; Zhu, T.; Wilms, M.; Gillies, G.; Lieberwirth, I.; Mittler, S.; Knoll, W; Kreiter, M. Langmuir 2005 21 12399

[17] Jin, R.; Cao, Y.; Mirkin, C. A.; Kelly, K. L.; Schatz, G. C.; Zheng, J. G. *Science* **2001**, *294*, 1901.

[18] Pastoriza-Santos, I.; Liz-Marzán, L. M. *Nano Lett.* **2002**, *2*, 903.

[19] Sun, Y.; Xia, Y. *Adv. Mater.* **2003**, *15*, 695.

[20] Millstone, J. E.; Park, S.; Shuford, K. L.; Qin, L.; Schatz, G. C.; Mirkin, C. A. *J. Am. Chem. Soc.* **2005**, *127*, 5312.

[21] Bastys, V.; Pastoriza-Santos, I.; Rodríguez-González, B.; Vaisnoras, R; Liz-Marzán, L. M. *Adv. Funct. Mater.* **2006**, *16*, 766.

[22] Sun, Y.; Xia, Y. *Science* **2002**, *298*, 2176.

[23] Kim, F.; Connor, S.; Song, H.; Kuykendall, T.; Yang, P. *Angew. Chem. Int. Ed.* **2004**, *43*, 3673.

[24] Im, S. H.; Lee, Y. T.; Wiley, B.; Xia, Y. *Angew. Chem. Int. Ed.* **2005**, *44*, 2154.

[25] Wiley, B. J.; Xiong, Y.; Li, Z.-Y.; Yin, Y.; Xia, Y. *Nano Lett.* **2006**, *6*, 765.

[26] Sánchez-Iglesias, A.; Pastoriza-Santos, I.; Pérez-Juste, J.; Rodríguez-González, B.; García de Abajo, F. J.; Liz-Marzán, L. M. *Adv. Mater.* **2006**, *18*, 2529.

[27] Rodríguez-Fernández, J.; Pérez-Juste, J.; Mulvaney, P.; Liz-Marzán, L. M. *J. Phys. Chem. B* **2005**, *109*, 14257.

[28] Grzelczak, M.; Pérez-Juste, J.; Rodríguez-González, B.; Liz-Marzán, L. M. *J. Mater. Chem.* **2006**, *16*, 3946.

[29] Pérez-Juste, J.; Rodríguez-González, B.; Mulvaney, P.; Liz-Marzán, L. M. *Adv. Funct. Mater.* **2005**, *15*, 1065.

[30] Correa-Duarte, M. A.; Pérez-Juste, J.; Sánchez-Iglesias, A.; Giersig, M.; Liz-Marzán, L. M. *Angew. Chem. Int. Ed.* **2005**, *44*, 4375.

[31] Pastoriza-Santos, I.; Pérez-Juste, J.; Liz-Marzán, L. M. *Chem. Mater.* **2006**, *18*, 2465.

[32] Liu, M.; Guyot-Sionnest, P. *J. Phys. Chem. B* **2005**, *109*, 22192.

[33] Khlebtsov, N. G.; Melnikov, A. G.; Bogatyrev, V. A.; Dykman, L. A.; Alekseeva, A. V.;

Trachuk, L. A.; Khlebtsov, B. N. *J. Phys. Chem. B* **2005**, *109*, 13578.

[34] Pelton, M.; Liu, M; Kim, H. Y.; Smith, G.; Guyot–Sionnest, P.; Scherer, N. F. *Optics Letters* **2006**, *31*, 2075.

[35] Pecora, R. *J. Chem. Phys.* **1968**, *49*, 1036.

[36] Broersma, S. *J. Chem. Phys.* **1960**, *32*, 1626. 1960!. 12 S.

[37] Broersma, S. *J. Chem. Phys.* **1960**, *32*, 1632.

[38] Ortega, A.; Garcia de la Torre, J. *J. Chem. Phys.* **2003**, *119*, 9914.

[39] Gao, J.; Bender, C. M.; Murphy, C. J. *Langmuir* **2003**, *19*, 9065.

[40] Nikoobakht, B.; El-Sayed, M. A., *Langmuir* **2001**, *17*, 6368.

[41] Tanford, C. *The Hydrophobic Effect*; Wiley: New York, 1973.

[42] van der Zande, B. M. I.; Dhont, J. K. G.; Böhmer, M. R.; Philipse, A. P. *Langmuir* **2000**, *16*, 459.

[43] Mie, G. *Ann. d. Phys.* **1908**, *25*, 377.

[44] Lord Rayleigh *Phil. Mag.* **1897**, *44*, 28.

[45] Pérez-Juste, J.; Pastoriza-Santos, I.; Liz-Marzan, L. M.; Mulvany, P. *Coord. Chem. Rev.* **2005**, *249*, 1870.

[46] Johnson, P. B.; Christy, R. W. *Phys. Rev. B* **1972**, *8*, 4370.

[47] Dhont, J. K. G. personal communication.